Increased depth of field through wave-front coding: using an off-axis zone plate lens with cubic phase modulation in an EUV microscope

Markus P. Benk*, Kenneth A. Goldberg, Iacopo Mochi, Weilun Chao, Erik H. Anderson
Lawrence Berkeley National Laboratory, 1 Cyclotron Road, Berkeley, CA 94720, USA

ABSTRACT

The authors are extending the capabilities of the *SHARP* microscope (SEMATECH High-NA Actinic Reticle review Project) by implementing wave front coding as a complementary imaging mode. *SHARP*, using a single off-axis lens has a tilted focal plane, reducing the instrument's field of view to a few micrometers. Wave-front coding increases the depth of field of an incoherent imaging system without affecting its resolution and light gathering power, rendering clear, large-field images for navigation and analysis. The resolution of the resulting image is close to the diffraction limit of the unmodified system. The authors have designed and nanofabricated zone plate lenses with a modified pattern that combines focusing power and wave front coding in a single optical element. The study clears the path to further applications of wave front coded zone plates in lab- and synchrotron-based microscopes and metrology tools. The authors have demonstrated wave-front coding in visible-light optical systems using Fresnel zone plate lenses in an off-axis configuration similar to *SHARP*. Simulations complementing the visible light experiments assess the performance of wave-front coded zone plates in the *SHARP* microscope.

Keywords: Wave front coding, cubic phase modulation, depth of focus, depth of field, EUV, microscopy, zone plate

1. INTRODUCTION

Wave front coding is a technique that increases the depth of field of an incoherent imaging system[1]. In addition to its focusing power the optical system modifies the phase of the received wave front. This phase modulation produces a disturbed image. Digital filtering is used to reconstruct an undisturbed image with nearly diffraction-limited resolution. The PSF (point-spread function) of the wave-front coded optical system is focus-independent over an extended depth of field. The increase in depth of field is achieved at the expense of some dynamic range. Wave-front coding is often implemented adding a phase mask to an imaging system.[1,2] For an optical system using a Fresnel zone plate lens, phase modulation and focusing power can be obtained from a single optical element encoding the phase modulation in the zone pattern.

SHARP is a newly commissioned synchrotron-based microscope designed for pattern and blank inspection on EUV-Lithography masks at 13.5 nm wavelength.[3] It uses high-magnification zone plate lenses in an off-axis configuration as imaging elements. The off-axis design causes the object plane to be tilted with respect to the flat, mask sample, leading to a focal gradient across the image with the center part of the field of view being in focus and the upper and lower parts being out of focus. The increased depth of field of the wave-front coded optical system covers the object plane within the microscope's field of view and therefore allows the reconstruction of an image that appears to be entirely in focus.

The focal length of a zone plate lens is strongly wavelength-dependent. This limits the acceptable spectral bandwidth of the illumination used with an imaging system. Sensitivity to wavelength-dependent misfocus or rather axial chromatic aberrations is significantly reduced in wave front coded optical system[2], thus allowing a higher spectral bandwidth of the illumination. Depending on the type of source in use, this may increase the throughput of a system and eliminate or reduce the requirements for lossy spectral filtering.

Wave-front coding is limited to incoherent optical systems[1]. In practice many optical systems are partially coherent. The illumination coherence factor σ is commonly used to describe the partial coherence in an optical system. It can be described as the ratio of the illumination divergence to the system's object sided NA (numerical aperture).[4] At a σ of 1 or above, the illumination is considered to be incoherent.

*mpbenk@lbl.gov; phone 1 510 486-5680; fax 1 510 486-4550; http://sharp.lbl.gov; www.cxro.lbl.gov

Photomask Technology 2013, edited by Thomas B. Faure, Paul W. Ackmann, Proc. of SPIE
Vol. 8880, 88801R · © 2013 SPIE · CCC code: 0277-786X/13/$18 · doi: 10.1117/12.2025954

SHARP's Fourier synthesis illuminator[3,4] allows continuous adjusting of the illumination partial coherence, thus allowing us to experimentally assess the requirements of wave-front coding in terms of partial coherence.

2. WAVE-FRONT CODING AND IMAGE RECONSTRUCTION

In this section the concept of wave-front coding and computational reconstruction of the undisturbed image are summarized.

2.1 Wave-front coding

The ambiguity function of the pupil function of an optical system contains the system's OTF (optical transfer function) with variable defocus[5]. The change in frequency response of the system for a given amount of defocus can be readily obtained from a plot of the ambiguity function. Using the ambiguity function, Dowski and Cathey have shown that the standard incoherent optical system with the cubic phase term

$$\phi = \alpha\left(X^3 + Y^3\right) \tag{1}$$

added to the pupil has a nearly constant OTF over a wide range of defocus[1]. $|X| \le 1$ and $|Y| \le 1$ are the normalized pupil coordinates. A typical value for the phase parameter α would be 20π. The OTF does not have zero values within its pass-band. Similar results can be obtained applying logarithmic[6] or polynomial[7] phase functions.

Figure 1 shows the PSFs of the incoherent optical system with and without cubic phase modulation calculated in focus and 4 waves out of focus. The reconstruction of the wave-front coded data is shown in column c. The model used for the calculation is discussed in section 4 of this paper. The cubic PSFs are not centered in the image to allow smaller graphics.

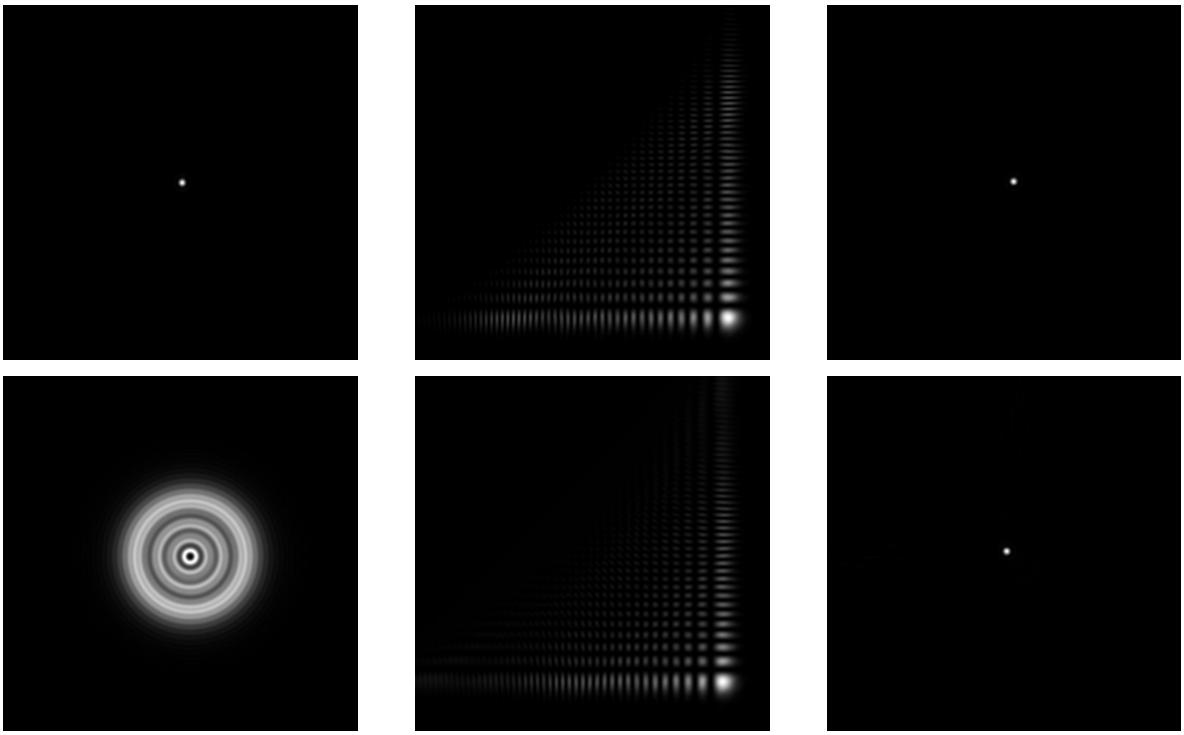

a b c

Figure 1. Calculated point-spread functions of the incoherent optical system; a) without cubic phase modulation, b) with cubic phase modulation and c) the reconstructions of b. Upper row is in focus, lower row is 4 waves out of focus

2.2 Image reconstruction

Reconstruction of the undisturbed image g from the wave-front coded image f can be done in the Fourier domain, multiplying its spectrum with a filter function H. The letter $\mathcal{F}$ represents the Fourier operator.

$$g = \mathcal{F}^{-1}\left(\mathcal{F}(f)\cdot H\right) \tag{2}$$

The filter function H is the ratio of the OTFs of the incoherent optical system with and without wave-front coding (WFC). It can be obtained from the corresponding PSFs, which can be measured or calculated.

$$H = \frac{\mathrm{OTF}_{\mathrm{WFC}}}{\mathrm{OTF}} = \frac{\mathcal{F}\left(\mathrm{PSF}_{\mathrm{WFC}}\right)}{\mathcal{F}\left(\mathrm{PSF}\right)} \tag{3}$$

3. ZONE PLATES

The SHARP microscope uses a variety of zone plate lenses with different numerical apertures and magnification. These are produced at the CXRO Nano-fabrication laboratory using electron beam lithography.

The border of the n-th zone in the off-axis zone pattern, with wave front coding, is described by equation 4.

$$\sqrt{p^2+x^2+y^2}+\sqrt{q^2+x^2+y^2} = p+q+n\cdot\frac{\lambda}{2}+\frac{\alpha}{k}\cdot\frac{x^3+\left(y-\Delta y\right)^3}{R^3} \tag{4}$$

This is the standard zone plate equation for point-to-point imaging with the cubic term added. p and q are the object distance and image distance. k is the wave number. x and y are the pupil coordinates. Since the zone plate is off-axis, the cubic term is centered with the center of the pupil at $x,y = 0,\Delta y$. R is the pupil radius.

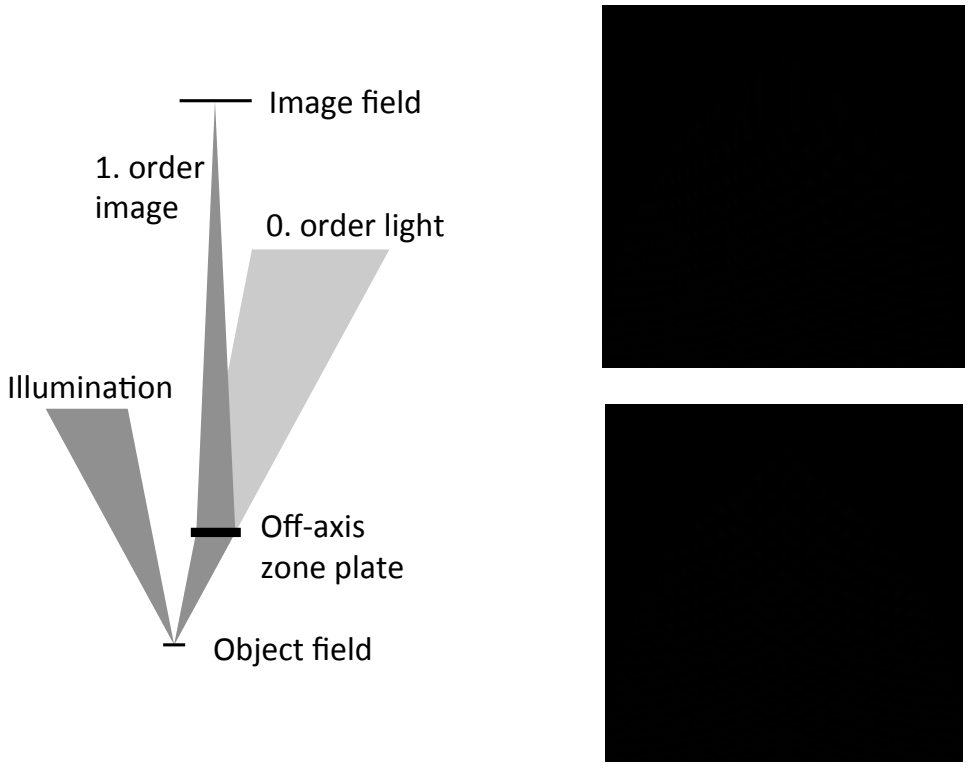

Figure 2. a) Ray path for zone plate in off-axis configuration.
b) Zone patterns for a phase parameter α of 15π (upper image) and 0 (lower image)

The ray path for the off-axis zone plate is illustrated in Figure 2a. Figure 2b shows two examples of zone patterns with a phase parameter α of 15π (upper image) and 0 (lower image). The latter corresponds to the standard off-axis zone plate.

Proof-of-principle experiments (described in Section 5) are carried out using off-axis zone plates designed for 632.8 nm wavelength. The zone plates are 1 mm in diameter and have 5 mm object distance and 50 mm image distance. The magnification is 10x. The zone plates are structured on a 0.5 mm thick quartz substrate using electron beam lithography. Chromium is used as the absorber.

4. SIMULATIONS

The MATLAB computing environment is used to model the EUV optical system of the SHARP-microscope. The simulation compares wave-front coded images to standard images in central and outer regions of the microscope's field of view. Incoherent and partially coherent models are discussed. In the incoherent model all points in the object plane are treated as individual point sources and propagated through the optical system sequentially. The model is used for the comparison to the unmodified system. The more complex and computationally more intensive, partially coherent model complements the study. The partially coherent image is calculated as the sum of fully coherent image of the object, using plane-wave illumination at varying angle of incidence. In the latter model, the field on the lens is calculated for the whole object at once and propagated to the image plane. The model corresponds to the image formation in the *SHARP*-microscope. Here, the spatially coherent synchrotron beam that illuminates the photo mask is scanned across a range of incidence angles to create arbitrary coherence properties. The model is used to investigate, whether a wave-front coded image, formed by the sum of fully coherent but mutually incoherent images allows reconstruction of the undisturbed image.

The configuration used for the simulation, given in Table 1, is one of the SHARP's commonly used configurations.

Table 1. Configuration of the SHARP microscope used for simulations.

Wavelength λ [nm]	Object distance p [mm]	Image distance q [mm]	Magnification M	Cubic parameter α	Numerical Aperture NA
13.5	0.5	450	900	$5\pi < \alpha < 30\pi$	0.0875

4.1 Incoherent model

The zone plate is modeled as a phase object with the pupil coordinates x and y centered with the aperture.

$$\psi = \begin{cases} e^{-ik\sqrt{p_0^2+x^2+(y+\Delta)^2}}\, e^{i\alpha\frac{x^3+y^3}{R^3}} & \sqrt{x^2+y^2} \le R \\ 0 & \sqrt{x^2+y^2} > R \end{cases} \tag{5}$$

The first exponent corresponds to the standard zone plate and the second exponent does the wave front coding. p_0 is the design object distance.

The field $E(u,v)$ at a point P in the object plane is propagated to the aperture and multiplied with ψ to obtain the field behind the lens $E(x,y)$.

$$E(x,y) = \frac{p}{i\lambda}\frac{1}{r^2} E(u,v)\cdot e^{ikr}\Delta u\Delta v\cdot\psi \tag{6}$$

In the simulation, the area of the unit cells in the object plane is given by $\Delta u\Delta v$. r is the varying distance from P to the zone plate aperture.

$$r = \sqrt{(x-u)^2+(y+\Delta-v)^2+p^2} \tag{7}$$

The Intensity I in the image of P is proportional to the Fourier transform of $E(x,y)$. The image of an extended object is obtained summing up the individual images of all points in the object plane.

$$I_{\text{Image}} \propto \sum_x \sum_y \left| \mathcal{F}(E(x,y)) \right|^2 \tag{8}$$

4.2 Field-dependent aberrations

The zone plate lenses used in *SHARP* are designed for point-to-point imaging. These lenses allow diffraction-limited imaging within a region 5 μm or smaller, depending on the numeral aperture. The microscope's visible field of view is about 30x30 μm^2, dictated by the magnification (900) and the size of the camera sensor (25.4-mm square). In addition to the focal gradient across the image, outer regions of the image field have significant aberrations. In the wave-front coded PSF, energy is distributed along the x- and y-axes. The field-dependent aberrations cause this distribution to stretch laterally, smearing the reconstructed image primarily in the x and y directions, asymmetrically. Figure 3 shows an aberrated off-center PSF of the unmodified optical system (a) and the reconstruction of the wave-front coded PSF (b). (The square root of (b) is shown in Figure 3c to increase the visibility of the tails.)

a b c

Figure 3. a) PSF of the unmodified optical system for an object point 15 μm off-center
b) Reconstruction calculated from the wave front coded PSF for an object point 15 μm off-center
c) Square root of b

We observe that the tails in the reconstruction of the wave-front coded PSF add constructively for features oriented in the x and y directions, degrading the image quality; whereas different orientations, not parallel to x and y, are not significantly affected.

a b

Figure 4. Simulated imaging of 100-nm half-pitch lines and spaces in vertical (a) and diagonal (b) orientations.

Figure 4 shows the reconstruction of wave-front coded images of 100 nm lines/spaces in simulation. Contrast in the vertical lines (a) decreases significantly along the pattern. Yet in a diagonal pattern (b), the tails do not degrade the image. Here, the modulation is higher and constant.

4.3 Results form the incoherent model

Different from biological imaging and other fields where wave-front coding has been applied, most features on EUV photo masks have *Manhattan geometry*, with patterns strongly oriented along grids in the *x* and *y* directions. Therefore, we predict that rotating the cubic phase term in the wave-front coding can significantly enhance the image reconstruction performance in *SHARP*. Here, our simulations are carried out with the cubic term rotated by 45° with respect to the mask coordinates.

Figure 5 shows a comparison of the simulation of horizontal 100 nm half-pitch lines/spaces imaged with and without wave-front coding. The simulation contains the center portion of the 30x30 μm^2 object field and five locations at its limits. Both configurations produce similar, high-quality images for the central pattern. At locations that are off-center in y, modulation is significantly reduced in the data from the unmodified system. This loss in modulation is dominated by defocus in upper and lower parts of the image caused by the focal gradient. Location 3 in figure 5 is off-center only in x. Although this location lies in the focal plane, modulation of the line patterns is significantly reduced for the unmodified system due to field-dependent aberrations. For features in Manhattan geometry, the wave-front coded system is less sensitive to the field-dependent aberrations resulting from *SHARP*'s single-lens, off-axis configuration. The individual simulations cover a region of approximately 1.46x1.46 μm^2 in the object plane. Lower intensities in the upper or lower line are caused by partial clipping in the object plane.

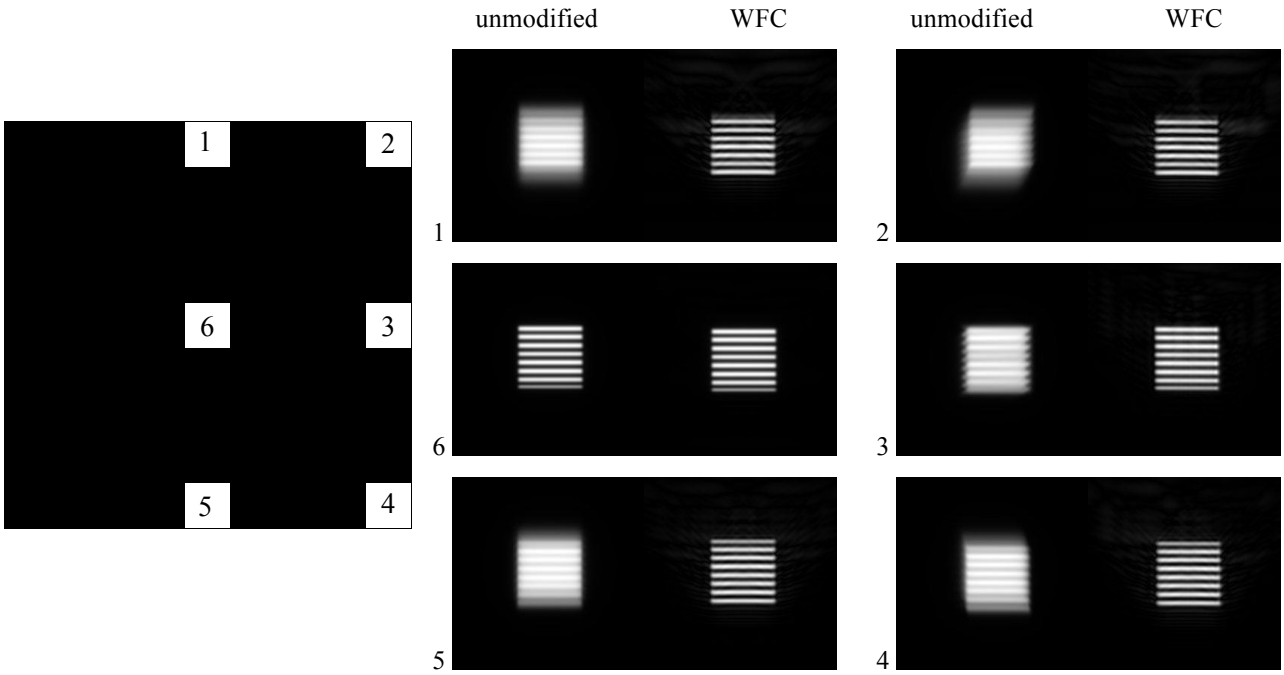

Figure 5. Simulated imaging of 100-nm half-pitch horizontal lines and spaces in 6 locations of *SHARP*'s 30x30 μm field of view: unmodified system and wave front coded optical system in comparison.

A significant part of SHARP's operation time is used for mask navigation. For this task, wave-front coding expands *SHARP*'s usable field of view to the entire sensor area increasing the efficiency of the tool. Mask navigation is seen as the main application of wave-front coding in *SHARP*. The applicability of the technique to tasks like pattern and defect inspection depends on the specific aim of the experiment. Future work aims at comparing properties like, e.g., critical dimension in aerial mask images recorded with and without wave-front coding.

4.4 Partially coherent model

Partially coherent imaging is simulated by calculating fully coherent images I_j of the object using plane-wave illumination. Each image is calculated at a different incidence angle of the illuminating plane wave with the range of angles covering the angular extend of the source to be modeled. The partially coherent image I_{pc} is obtained by incoherently summing the images I_j.

$$I_{pc} = \sum_j I_j \tag{9}$$

The coherent images are calculated by Fourier-transforming the field behind the lens $E(x,y)$.

$$I_j \propto \left| \mathcal{F}(E(x,y)) \right|^2 \tag{10}$$

In contrast to the incoherent model, the field behind the lens is calculated summing up the contributions of all object points in the zone plane aperture and multiplying with ψ.

$$E(x,y) = \psi \cdot \frac{p}{i\lambda} \cdot \Delta u \Delta v \sum_u \sum_v \frac{1}{r^2} E(u,v) \cdot e^{ikr} \tag{11}$$

The object field is defined multiplying the incident plane wave at the angles θ_u and θ_v with the local reflection or transmission coefficient of the object $\Gamma(u,v)$, in this case the reflectivity coefficient of the photo mask.

$$E(u,v) = E_0 \cdot e^{ik(u\sin\theta_v + v\sin\theta_u)} \cdot \Gamma(u,v) \tag{12}$$

A σ of 1 is used for the partially coherent simulation. The result (a) is compared to the incoherent model (b) in figure 6. Both datasets show similar modulation. The lines are slightly wider in the partially coherent model. The reconstruction function H (Eq. 3) is identical for both the coherent and incoherent model. The limited number of illumination angles in the partially coherent model is a potential reason for the observed difference. The successful reconstruction for σ=1 indicates the applicability of wave-front coding to *SHARP* using a σ of 1 for the illumination. The influence of different coherence settings on the performance of wave-front coding will be experimentally investigated using *SHARP*'s Fourier synthesis illuminator.

a b

Figure 6. Imaging of 100 nm horizontal lines and spaces calculated from the partially coherent model for σ=1 (a) and incoherent model (b).

5. VISIBLE LIGHT EXPERIMENT

Visible light experiments are carried out to complement the simulation results. A bright elbow-pattern with 4 μm lines and spaces (8 nm per cycle) on an absorber-covered glass substrate is imaged in transmission-mode. A frequency-doubled Nd:YAG laser with 632.8 nm wavelength is used for sample illumination. To break the spatial coherence of the light, the expanded beam is sent to a rotating ground-glass disk acting as a secondary source. The image is recorded using a CCD sensor with 4.4-μm pixel size. The Rayleigh-resolution of the setup is 3.86 μm. The 4 elbows cover a region of approximately 300 μm by 400 μm in the object plane. The angular extension of the object plane corresponds to 150 μm over 5000 μm focal length. This ratio matches the 15 μm over 500 μm in the SHARP microscope. The numerical aperture of 0.1 exceeds the 0.0875 used in the simulations.

Figure 7 shows the results of the visible light experiments. Images a and b are recorded without cubic phase modulation. In image a, the upper elbows are in focus. In image b the lower elbows are in focus. Due to the tilted focal plane of the off-axis configuration, the lower elbows in image a and the upper elbows in image b are significantly blurred. Image c is recorded with cubic phase modulation of $\pm 10\,\pi$ across the aperture. The reconstruction of image c is shown in image d; the whole image appears to be in focus. The pattern is resolved across the image at a modulation exceeding the modulation in the out-of-focus regions of images a and b.

The wave-front coded zone plate's cubic phase term has 0° rotation with respect to the x/y-axis. The reconstructed data shows some artifacts caused by field-dependent aberrations, particularly in the 0°/90° elbows. Patchy illumination and stray-light are possible sources of non-uniformity in the absorber region surrounding the elbows. The data supports the use of cubic phase modulation in the *SHARP* microscope. An improved quality of the reconstructed images is sought for the EUV implementation of wave-front coding.

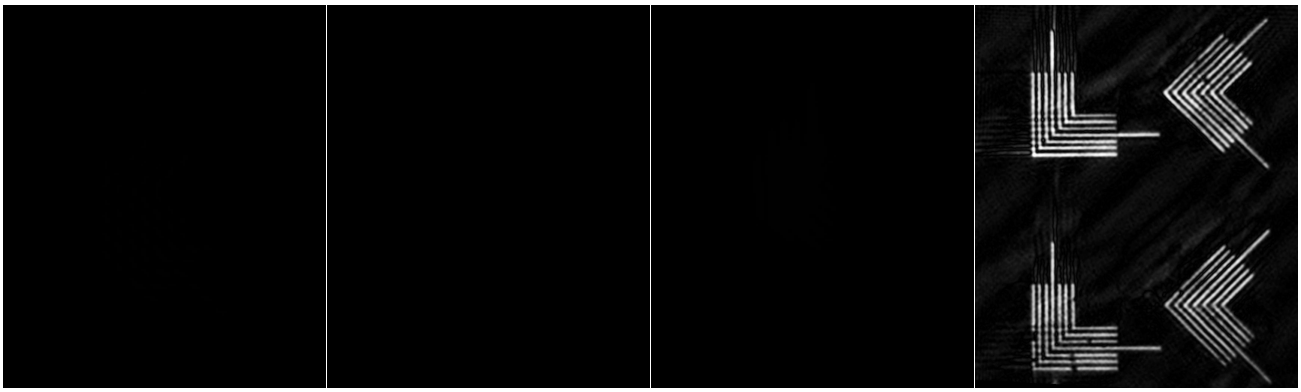

a b c d

Figure 7. Visible light images of elbow pattern with 4 μm lines/spaces, recorded using off-axis zone plate lenses
a) Without cubic phase modulation, upper elbows in focus
b) Without cubic phase modulation, lower elbows in focus
c) With cubic phase modulation, $\alpha=10\pi$
d) Reconstruction of c

6. SUMMARY

Wave-front coding will be added to the *SHARP* microscope as a complementary imaging mode for increased depth of field. *SHARP*, using a single off-axis lens has a tilted focal plane, reducing the instrument's field of view to a few micrometers. Wave-front coding eliminates the focal gradient across the instruments image plane, thus enabling sharp imaging across its 30x30 μm^2 field of view. Reconstruction of the undisturbed image in the Fourier domain only takes a fraction of a second, thus allowing real-time mask navigation.

The authors have designed and nanofabricated zone plate lenses with a modified pattern that combines focusing power and wave front coding in a single optical element. Visible light experiments are carried out using Fresnel zone plate

lenses with cubic phase modulation in an off-axis configuration that is similar to *SHARP*. A wave-front coded image of an elbow-pattern is recorded and the unmodified image is digitally reconstructed.

Simulations are carried out to evaluate the performance of wave-front coding in the *SHARP* microscope. For imaging Manhattan-like geometries, the simulation shows a significant reduction in sensitivity to field-dependent aberrations for the wave-front coded optical system with a 45° rotated cubic term. A model including spatial coherence shows successful reconstruction of wave-front coded images at an illumination coherence factor σ of 1, thus underlining the applicability of the technique to *SHARP*.

The study shows that wave-front coding has the potential to overcome some of the limitations of single-lens on- and off-axis imaging systems.

7. ACKNOWLEDGEMENT

This work was performed by University of California Lawrence Berkeley National Laboratory under the auspices of the U.S. Department of Energy. Funding by SEMATECH under Contract No. DE-AC02-05CH11231 is gratefully acknowledged.

8. REFERENCES

[1] Dowsky, E. R. and Cathey W. T., "Extended depth of field through wave-front coding," APPLIED OPTICS 34 (11), 1859-1866 (1995).
[2] Wach, H. B, Dowski E. R. and Cathey W. T., "Control of chromatic focal shift through wave-front coding," APPLIED OPTICS 37 (23), 5359-5367 (1998).
[3] Goldberg, K. A. et. al., "Comissioning an EUV mask microscope for lithography generations reaching 8 nm," Proc. SPIE 8679, 867919 (2013).
[4] Naulleau, P. P., Goldberg, K. A., Batson, P., Bokor, J., Denham, P and Rekawa, S, "Fourier-synthesis custom-coherence illuminator for extreme ultraviolet microfield lithography," APPLIED OPTICS 42 (5), 820-826 (2003).
[5] Brenner, K.-H., Lohmann, A. W. and Ojeda-Castaneda, J., "The ambiguity function as a polar display of the OTF," OPTICS COMMUNICATIONS 44 (5), 323-326 (1983).
[6] Sherif, S. S., Cathey W. T. and Dowski E. R., "Phase plate to extend the depth of field of incoherent hybrid imaging systems," APPLIED OPTICS 43 (13), 2709-2721 (2004).
[7] Caron, N. and Sheng, Y., "Polynomial phase masks for extending the depth of field of a microscope," APPLIED OPTICS 47 (22), E39-E43 (2008).